THE JOURNAL OF BIOLOGICAL CHEMISTRY VOL. 282, NO. 38, pp. 27754–27759, September 21, 2007
Printed in the U.S.A.

Cryoelectron Tomographic Analysis of an HIV-neutralizing Protein and Its Complex with Native Viral gp120*[S]

Received for publication, March 8, 2007, and in revised form, June 1, 2007 Published, JBC Papers in Press, June 28, 2007, DOI 10.1074/jbc.M702025200

Adam Bennett[‡§1], Jun Liu[‡], Donald Van Ryk[¶], Donald Bliss[‖], James Arthos[¶], Robert M. Henderson[§], and Sriram Subramaniam[‡2]

From the [‡]Laboratory of Cell Biology, NCI, [¶]Laboratory of Immunoregulation, NIAID, and [‖]Audiovisual Program Development Branch, National Library of Medicine, National Institutes of Health, Bethesda, Maryland 20892 and [§]Department of Pharmacology, University of Cambridge, Cambridge CB2 1PD, United Kingdom

Identifying structural determinants of human immunodeficiency virus (HIV) neutralization is an important component of rational drug and vaccine design. We used cryoelectron tomography and atomic force microscopy to characterize the structure of an extremely potent HIV-neutralizing protein, D1D2-Igαtp (abbreviated as D1D2-IgP), a polyvalent antibody construct that presents dodecameric CD4 in place of the Fab regions. We show that D1D2-IgP has a novel structure, displaying greater flexibility of its antibody arms than the closely related IgM. Using simian immunodeficiency virus in complex with D1D2-IgP, we present unequivocal evidence that D1D2-IgP can cross-link surface spikes on the same virus and on neighboring viruses. The observed binding to the viral envelope spikes is the result of specific CD4-gp120 interaction, because binding was not observed with MICA-IgP, a construct that is identical to D1D2-IgP except that major histocompatibility complex Class I-related Chain A (MICA) replaces the CD4 moiety. CD4-mediated binding was also associated with a significantly elevated proportion of ruptured viruses. The ratio of inactivated to CD4-liganded gp120-gp41 spikes can be much greater than 1:1, because all gp120-gp41 spikes on the closely apposed surfaces of cross-linked viruses should be incapable of accessing the target cell surface and mediating entry, as a result of inter-virus spike cross-linking. These results implicate flexibility rather than steric bulk or polyvalence *per se* as a structural explanation for the extreme potency of D1D2-IgP and thus suggest polyvalence presented on a flexible scaffold as a key design criterion for small molecule HIV entry inhibitors.

Human immunodeficiency virus type 1 (HIV-1)[3] infection of target cells is initiated by binding of the viral envelope glycoprotein gp120 to the cell surface receptor CD4 (1–3). The first step in the infection process, gp120-CD4 binding is an attractive drug target because the CD4 binding site of gp120 is well conserved and because *de novo* infection of target cells would be blocked, preventing all subsequent stages of the viral life cycle. No therapeutic agents that target gp120-CD4 binding are currently available, although certain small molecules are in clinical trials (reviewed in Ref. 4).

Soluble monomeric CD4 (sCD4) neutralizes primary isolates poorly at pharmacologically realizable concentrations (5) and is therefore not useful as a therapeutic agent against HIV-1. Minimally passaged clinical primary isolates, which best model the *in vivo* virus, are unaffected by physiologically sustainable concentrations of sCD4 in infectivity assays (6). Recent reports suggest that the sCD4-induced conformational fixation in gp120 (7–9) makes sCD4 binding energetically unfavorable (6).

In contrast to the soluble monomeric form, CD4 on the cell surface is thought to be clustered (10, 11). The clustered CD4 may mediate an avidity effect, so that soluble CD4 competes poorly with target cell CD4 for viral gp120 (6). To mimic the clustering of cell surface CD4, Arthos *et al.* (12) designed a multimeric CD4 construct, D1D2-Igαtp (which we abbreviate as D1D2-IgP, where "P" indicates the tendency of this construct to polymerize), achieving a similar avidity effect. D1D2-IgP is a multidomain protein that comprises the two extracellular N-terminal domains of human CD4, D1 and D2, fused to the hinge, Cγ2, and Cγ3 domains of human IgG1, fused in turn to the 18-amino acid human IgA α secretory tailpiece. The α secretory tailpiece promotes disulfide-mediated immunoglobulin multimerization. Analytical ultracentrifugation and dynamic light scattering revealed that D1D2-IgP molecules are typically multimeric species that carry 6–8 or more $Ig_2(CD4)_2$ units (*i.e.* 12–14 CD4 units) and have sizes ranging from ~600 to ~1200 kDa, with a 12-nm average hydrodynamic radius (12). D1D2-IgP neutralizes minimally passaged primary clinical isolates of HIV-1 at <3 nM IC_{90} values (6, 12), lower than those reported of monoclonal antibodies, polyclonal sera, or other CD4 constructs (6, 13, 14).

It has been hypothesized that the steric bulk of D1D2-IgP, which is many times larger than a monoclonal antibody, prevents approach and binding of gp120 to target cell CD4 (12). However, the large mass of D1D2-IgP is also a disadvantage, as it would likely result in undesirable pharmacologic properties such as poor distribution and immunogenicity. Here, we undertook to understand the structural basis of D1D2-IgP neutraliza-

* This work was supported in part by the intramural program of the NCI, National Institutes of Health. The costs of publication of this article were defrayed in part by the payment of page charges. This article must therefore be hereby marked "*advertisement*" in accordance with 18 U.S.C. Section 1734 solely to indicate this fact.

[S] The on-line version of this article (available at http://www.jbc.org) contains supplemental Fig. S1 and Movies M1–M9.

[1] Supported by the National Institutes of Health/University of Cambridge Graduate Partnerships Program and the Winston Churchill Foundation scholarship.

[2] To whom correspondence should be addressed: Laboratory of Cell Biology, NCI, National Institutes of Health, Bldg. 50, Rm. 4306, 50 South Dr., Bethesda, MD 20892-8008. Tel.: 301-594-2062; Fax: 301-480-3834; E-mail: ss1@nih.gov.

[3] The abbreviations used are: HIV-1, human immunodeficiency type virus 1; AFM, atomic force microscopy; HBS, HEPES-buffered saline; MICA, major histocompatibility complex class I-related chain A; SIV, simian immunodeficiency virus; TBS, Tris-buffered saline; IgM, immunoglobulin molecule.

tion of HIV using cryoelectron tomography and solution atomic force microscopy (AFM) in order to inform rational design of therapeutic agents that block gp120-CD4 binding and that possess both desirable pharmacologic properties and key structural determinants of potency.

EXPERIMENTAL PROCEDURES

Protein Expression and Purification—D1D2-IgP was expressed and purified as described (12), with modifications. Briefly, the published procedure was followed by fractionation over a Superose 6 size exclusion column (Amersham Biosciences) in HEPES-buffered saline (HBS), and the peak fraction was collected. The same procedure was used in the preparation of MICA-IgP, which carries major histocompatibility complex class I-related chain A (MICA) in place of D1 and D2 domains of CD4.

Preparation of Purified SIV—Simian immunodeficiency virus (SIV) strain mac239 that had been purified (15) and CD45-depleted to remove microvesicles (16) and inactivated with Aldrithiol-2, which preserves the envelope proteins (17), was kindly provided by Jeff Lifson (Science Applications International Corp., Frederick, MD).

Cryoelectron Tomography—Purified viral suspensions were mixed with either a solution of HBS, pH 7.4, or an equal volume of 600 μg/ml D1D2-IgP or MICA-IgP in HBS, immediately and without incubation deposited on Quantifoil grids (Quantifoil Inc., Jena, Germany) and plunge-frozen using a Vitrobot device (FEI Co.). Grids were imaged at liquid nitrogen temperatures and 6-μm defocus, $\times$34,000 magnification, using a Polara field emission gun electron microscope (FEI Co.) operated at 300 kV, equipped with a GIF 2000 2K $\times$ 2K CCD camera placed at the end of a Gatan energy filter (Gatan, Inc., Pleasanton, CA). Isolated D1D2-IgP, immunoaffinity-purified human IgM (Upstate Cell Signaling Solutions, Waltham, MA), or MICA-IgP were imaged in the same way except that holey carbon grids were used. All tilt series for tomographic reconstruction were acquired using the FEI tomography software package Xplore3D in the range $\pm$ 70°, using the Saxton tilt scheme with 3° initial tilt increment, aligned without fiducial markers using Protomo (18), and reconstructed using weighted back projection as implemented in Protomo for isolated proteins and Serial Iterative Reconstruction Technique as implemented in the Inspect3D software (FEI Co.) in all other cases. Visualization was carried out using software tools implemented in the program Amira (TGS, San Diego, CA).

Solution Atomic Force Microscopy—A solution of D1D2-IgP, IgM, or MICA-IgP in 50 mM Tris-buffered saline (TBS), pH 7.4, was deposited on freshly cleaved mica coated with poly-L-lysine (Sigma), incubated for 15 min, rinsed three times with TBS, and imaged in TBS in tapping mode on a Digital Instruments MultiMode atomic force microscope (Veeco, Santa Barbara, CA) with a Veeco NP-S scanning probe.

Air Atomic Force Microscopy—An IgM solution of 3.3 μg/ml protein in 50 μl of TBS was incubated on poly-L-lysine-coated mica for 2 min at room temperature, followed by rinsing with 2 ml of 0.1$\times$ TBS and drying under nitrogen. A D1D2-IgP solution of 4.73 μg/ml protein in 50 μl of TBS was incubated on poly-L-lysine-coated mica at room temperature for 10 min, followed by rinsing with 10 ml of Milli-Q water and drying under nitrogen. Uranyl acetate pretreatment was performed by incubation of 50 μl of protein in TBS on freshly cleaved mica for 2 min at room temperature, followed by rinsing twice with 1 ml of 0.1$\times$ TBS. This was followed by mixing of the meniscus with 100 μl of 1% uranyl acetate. The sample was dried to a thin film by application of the inverted sample to a piece of filter paper, followed by drying under nitrogen. Images were acquired in air tapping mode on a Digital Instruments MultiMode atomic force microscope (Veeco) with a SuperSharp silicon scanning probe (NanoSensors, Neuchatel, Switzerland).

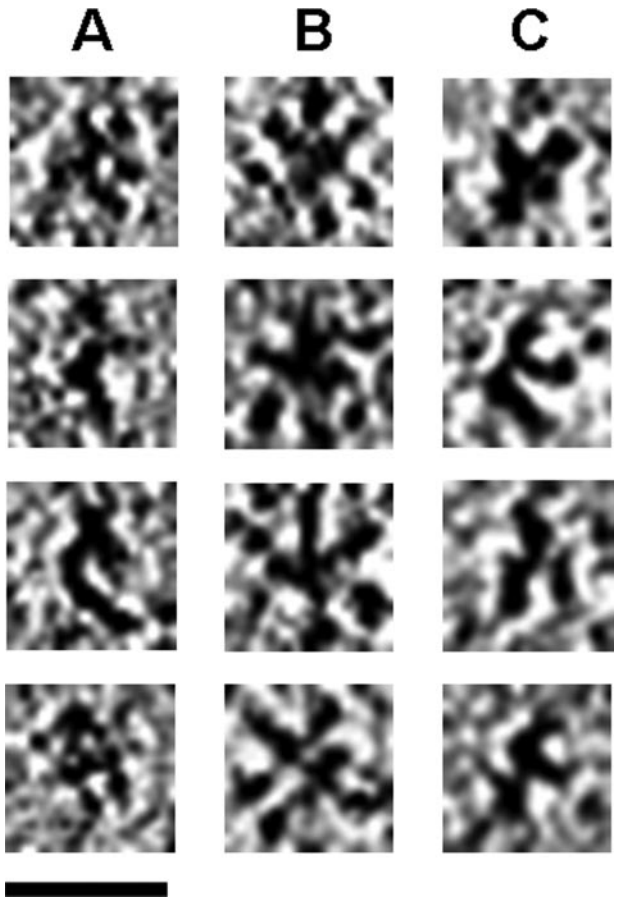

FIGURE 1. **Comparison of D1D2-IgP, IgM, and MICA-IgP structures by cryoelectron tomography.** Tomographic slices (0.82-nm thickness) of individual D1D2-IgP(*A*), IgM (*B*), and MICA-IgP (*C*) molecules in vitreous ice, from tilt series recorded at 300 kV and reconstructed using weighted back projection. *Scale bar*, 30 nm.

RESULTS

D1D2-IgP is a multimeric CD4-immunoglobulin fusion construct with exemplary neutralization activity against primary isolates of HIV-1 (6, 12). We imaged the three-dimensional structure of individual unfixed, unstained D1D2-IgP particles in vitreous ice using cryoelectron tomography. As shown in tomographic slices and threshold segmentations of selected molecules (Fig. 1*A*, Fig. 2, *A* and *B*, and supplemental Movie M1), D1D2-IgP particles ranged in width from 20–35 nm, with an average diameter of ~25 nm. Inspection of the three-dimensional structures shows that the putative $Ig_2(CD4)_2$ units, or arms, are flexible, neither arranged in a radial pattern nor

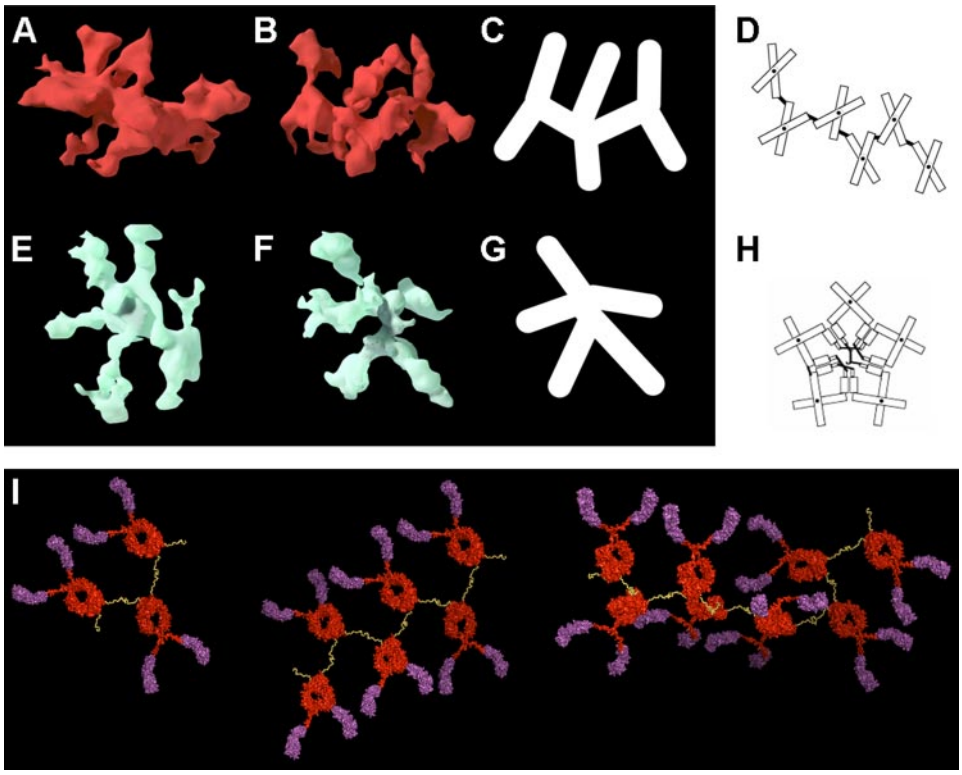

FIGURE 2. **D1D2-IgP and IgM are assembled differently.** *A* and *B*, three-dimensional automatic density threshold segmentation of individual D1D2-IgP molecules in vitreous ice, with color applied. *C*, schematic representation of the domain organization of D1D2-IgP molecules observed in tomographic structures like those shown in *panels A* and *B*. *D*, model of D1D2-IgP immunoglobulin assembly, mediated by the α secretory tailpiece. Each *white bar* represents a D1D2-IgP polypeptide chain, two of which form the $Ig_2(CD4)_2$ unit, or arm. The *black dots* represent inter-chain disulfide bonds at the immunoglobulin hinge domain; the *black bars* represent inter-arm disulfide bonds at the α tailpiece. D1D2-IgP can have from 3 to 8 or more arms; a hexamer is shown in this example. *E* and *F*, three-dimensional automatic density threshold segmentation of individual IgM molecules in vitreous ice, with color applied. *G*, schematic representation of the domain organization of IgM molecules observed in tomographic structures like those shown in *panels E* and *F*. *H*, schematic of IgM structure, adapted from Fazel *et al.* (25), with permission. Each long *white bar* represents a Cμ2–Cμ3 portion of the μ polypeptide chain, two of which form an arm. Each short *white bar* represents a Cμ4 tail. The *black dots* represent inter-chain disulfide bonds at the immunoglobulin hinge domain; the *black bars* represent inter-arm disulfide bonds at the Cμ3 or Cμ4 domain. The letter "J" in the center of the schematic in panel *H* represents the J chain. IgM can exist as a pentamer and as a hexamer; a pentamer is shown. *I*, hypothetical molecular model of the D1D2-IgP trimer (*left*), hexamer (*center*), and nonamer (*right*). The CD4 domains are colored *magenta*, the IgG domains *red*, and the α secretory tailpieces *yellow-orange*. The models are constructed from the x-ray crystal structure coordinates of soluble CD4 (28), IgG b12, (29), and a model of the IgA α secretory tailpiece (30). The models were created using PyMol.

largely confined to an annulus (Fig. 2*C*). For purposes of comparison, we also carried out cryoelectron tomographic analysis of two related specimens using identical imaging conditions: the pentameric immunoglobulin molecule IgM and MICA-IgP, in which the CD4 domains in D1D2-IgP have been substituted by MICA, a moiety of similar mass that does not bind gp120 but that belongs to the same structural superfamily as CD4. MICA is a ligand for the NKG2D receptors on natural killer cells (19), which is not expressed by the cell lines used to produce viruses used in this study. IgM particles, which ranged in maximum diameter from 30–33 nm, were typically less flexible, with planar, radially oriented arms frequently resolved (Fig. 1*B*, Fig. 2, *E–G*, and supplemental Movie M2), as expected based on the known structure (reviewed in Ref. 20). However, MICA-IgP molecules, which have the same structural scaffold as D1D2-IgP, displayed random orientation of the arms as observed for D1D2-IgP (Fig. 1*C* and supplemental Movie M3).

We also imaged the topographical morphologies of D1D2-IgP, IgM, and MICA-IgP absorbed to a mica surface in air and in aqueous buffer, using AFM. D1D2-IgP and MICA-IgP typically displayed a varied, elongated morphology, whereas IgM displayed a uniformly circular morphology (supplemental Fig. S1). The AFM micrographs, which are isoforce surfaces and not true three-dimensional data, do not necessarily provide a faithful description of the native state molecular morphology, because apparent structures are potentially affected by variability in the manner of absorption to the mica and by preferential absorption of certain species. For the same reason, however, the greater morphological variability observed for D1D2-IgP implies a greater number of absorption conformations and thus greater flexibility than IgM. The apparent sizes of these particles imaged by AFM, unlike the morphologies, are not meaningful due to the effect of tip sample convolution (reviewed in Ref. 21).

Next we obtained cryoelectron tomograms of SIV virions in the absence and presence of MICA-IgP or D1D2-IgP. We imaged virions of SIV strain mac239, selected because of the high levels of envelope glycoprotein incorporation in the membranes of these virions (22–24). Consistent with these previous electron microscopic analyses, the typical SIV virion is 120 nm in diameter and can be studded with as many as 100 envelope spikes of ~13 nm in height, and ~12 nm wide at the distal end (Fig. 3, *A* and *D*). Virions treated with D1D2-IgP showed additional densities attached to the envelope spikes with sizes similar to D1D2-IgP (Fig. 3, *C* and *E*, and supplemental Movie M4), with two or more domains engaging envelope spikes within or between virions (Fig. 4 and supplemental Movies M5–M8). Neither buffer-treated SIV (650 viral tomograms) nor MICA-IgP-treated SIV (321 viral tomograms) displayed any additional density bound to an envelope spike (Fig. 3*B* and supplemental Movie M9). We conclude that the observed additional densities in the sample treated with D1D2-IgP are likely to represent individual D1D2-IgP molecules bound to the envelope spikes of SIV. Because MICA-IgP differs from D1D2-IgP only in specificity for gp120, this binding must be mediated by specific interaction of CD4 moieties with gp120 on the surface of SIV viruses.

Besides the presence of additional densities on the surface of the virus, the most striking difference observed in D1D2-IgP-

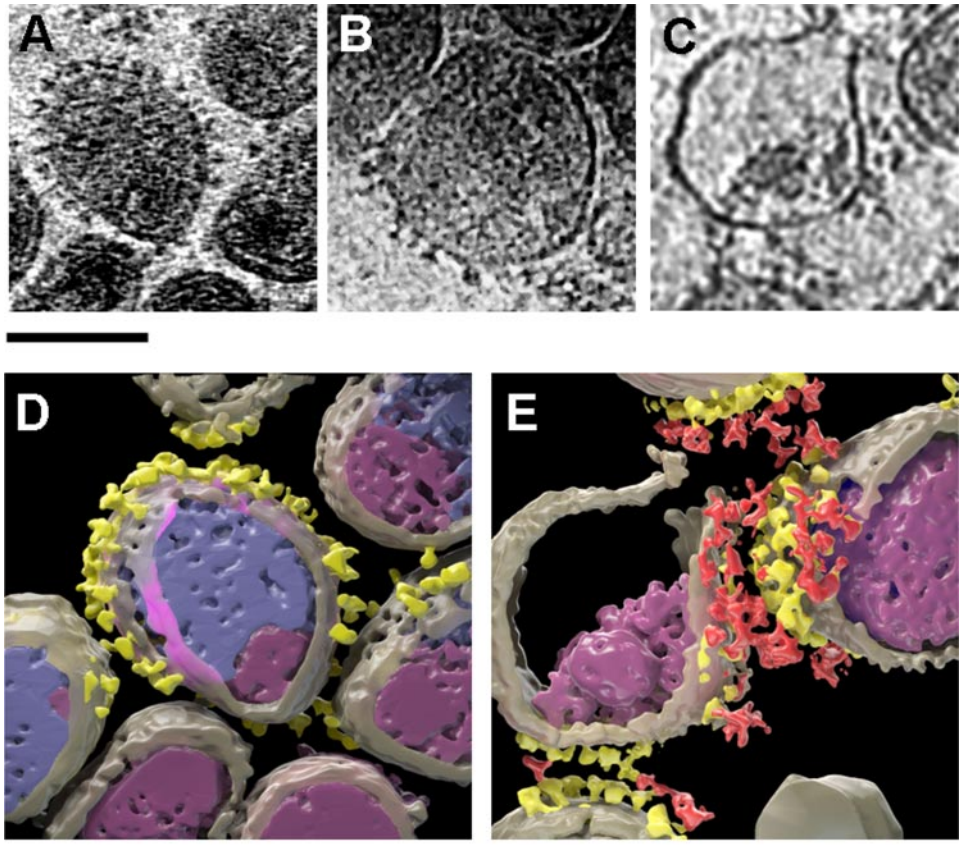

FIGURE 3. **Direct visualization of SIV neutralization.** Cryoelectron tomographic slices (thickness 8.2 nm, *panels A–C*) and three-dimensional automatic density threshold segmentations (*D* and *E*), with color applied, of untreated (*A* and *D*), MICA-IgP-treated, and D1D2-IgP-treated (*C* and *E*) SIV virions in vitreous ice, from tilt series recorded at 300 kV and reconstructed using weighted back-projection. *Red*, D1D2-IgP; *Yellow*, Spike; *Gray*, Membrane; *Purple*, Core; *Blue*, Matrix. *Scale bars*, 100 nm.

treated and control samples was an increase in proportion of ruptured virions (Fig. 5). Here, we define a ruptured virion as one showing an obvious membrane breach and total or partial loss of contents. These features were often accompanied by a reversal of membrane curvature near the opening, creating a small neck-like region. To quantitate the extent of rupture induced by addition of D1D2-IgP to the virions, we carried out a series of four independent replicates (including controls for each set). Treatment of SIV with D1D2-IgP in HBS was correlated with 25.4 ± 3.7% virion rupture (n = 2,126 virions; four replicates). Treatment of another portion of the same aliquot of SIV with the same concentration of MICA-IgP in an equal volume of HBS buffer was correlated with 9.8 ± 2.6% virion rupture (n = 2,881 virions; four replicates); treatment of another portion of the same aliquot with an equal volume of HBS buffer alone was correlated with 10.6 ± 2.1% virion rupture (n = 2,253 virions; four replicates). This corresponds to $X^2 = 216$ and $p < 0.001$ for D1D2-IgP *versus* an equal concentration of MICA-IgP in an equal volume of HBS, and $X^2 = 163$ and $p < 0.001$ for D1D2-IgP *versus* an equal volume of HBS, both added to a separate portion of the same aliquot for each replicate. For MICA-IgP in HBS *versus* an equal volume of HBS alone, $X^2 = 0.9$, $p \leq 1$. There is no significant difference in virion rupture between MICA-IgP in HBS and an equal volume of HBS alone, as expected. Because for each replicate each sample was made in parallel using the same aliquot and the same buffer and concentration, hidden variables potentially influencing virion rupture acted identically on each sample, and so we conclude that CD4-mediated binding of D1D2-IgP to SIV is correlated with a significant increase in virion rupture.

DISCUSSION

We show here that D1D2-IgP, a multimeric CD4-immunoglobulin construct with extreme neutralization activity against primary isolates of HIV-1 (6, 12), is heterogeneous in size and structure. Cryoelectron tomography studies reveal that the monomer units, or arms, of D1D2-IgP appear to have no preferred orientation, in contrast to those of IgM imaged under identical conditions. The apparent orientational variability of the D1D2-IgP arms compared with the IgM arms and the greater morphological variation in surface-absorbed D1D2-IgP molecules imaged by AFM imply that D1D2-IgP is more flexible than IgM, which is not surprising given that IgM domains are multimerized by two intermolecular disulfide bonds, which may be thought of as a bridge, whereas D1D2-IgP domains are linked by only one, which might function more like a hinge (Fig. 2, *D*, *H*, and *I*). The IgM schematic in Fig. 2*H* is adapted from Fazel *et al.* (25), with permission.

We have directly visualized specific CD4-mediated binding of D1D2-IgP to SIV virions and viral rupture correlated with this binding. The discovery of virion rupture correlated with D1D2-IgP binding is unexpected. Although the mechanism of rupture is not clear, one possibility is that the geometric constraints of gp120 to remain membrane-associated and bound to D1D2-IgP may lead to membrane destabilization and leakage of contents. Observation of virion rupture implies that the ratio of inactivated to CD4-liganded spikes could be much greater than 1:1, because rupture presumably neutralizes the infectivity of a virion and thereby the ability of its spikes to mediate infection.

D1D2-IgP appears to bridge neighboring spikes both within and between virions, highlighting the importance of avidity in effective neutralization of HIV. Intra-virion spike cross-linking may disable the function of the bound spikes due to the steric bulk of the D1D2-IgP molecule, which was proposed as a hypothetical neutralization mechanism of this construct (12), and of a similar CD4 construct based on two-dimensional electron micrographs of negatively stained complexes with soluble monomeric recombinant gp120 (26). In addition to direct demonstration of this proposal of spike cross-linking on the same virion, we demonstrate here that D1D2-IgP can cross-link

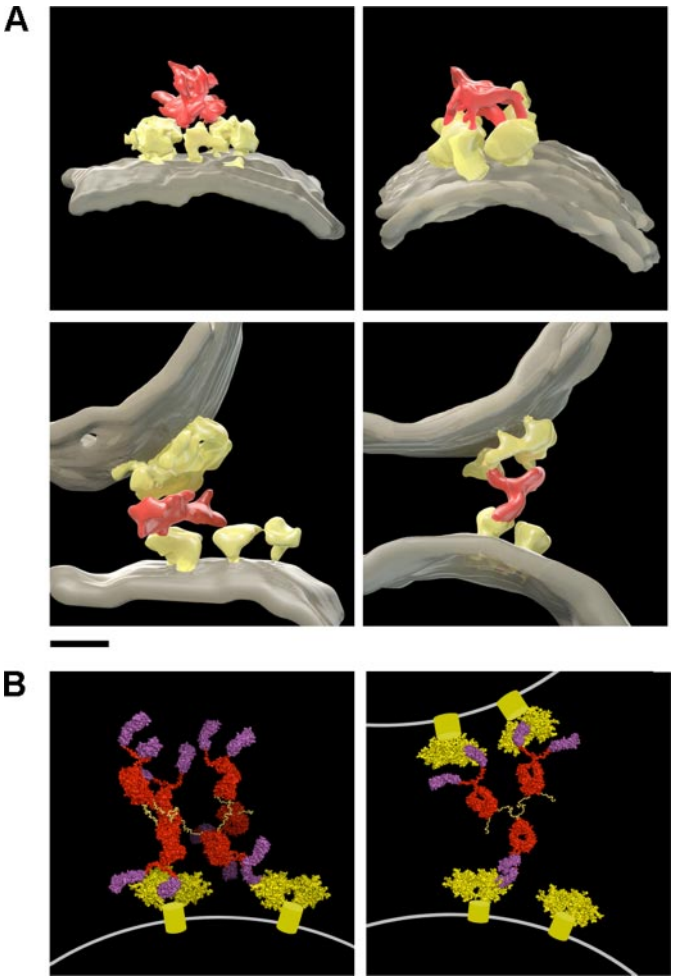

FIGURE 4. **CD4-neutralized viral gp120.** *A*, three-dimensional automatic density threshold segmentation of individual D1D2-IgP-SIV complexes in vitreous ice, with color applied, from tilt series recorded at 300 kV. *Red*, D1D2-IgP; *Yellow*, Spike; *Gray*, Membrane. Tomograms of the complexes shown at *upper left*, *upper right*, *lower left*, and *lower right* are shown in supplemental Movies M5, M6, M7, and M8, respectively. *Scale bar*, 15 nm. *B*, hypothetical molecular models of intra-virion (*left*) and inter-virion (*right*) spike cross-linking by D1D2-IgP. In the D1D2-IgP molecules, the CD4 domains are colored *magenta*, the IgG domains *red*, and the α secretory tailpieces *yellow-orange*. The gp120 trimers are colored *yellow*. The models are constructed from the x-ray crystal structure coordinates of soluble CD4 (28), IgG b12 (29), a model of the IgA α secretory tailpiece (30), and a model of the CD4- and 17b-liganded gp120 trimer (31). CD4 domains that are not part of a D1D2-IgP molecule are not shown; 17b is not shown. The models were created using PyMol. The *gray surface* represents the viral membrane. The *yellow cylinders* represent gp41, for which a pre-fusion structure is not available.

spikes on neighboring virions. This appears to bring virions into close apposition as a result of the cross-linking, potentially increasing the ratio of inactivated spikes to CD4-bound spikes above 1:1, because all spikes on the apposed membranes of cross-linked virions should be incapable of accessing the cell surface. This combination of intra- and inter-virion spike cross-linking offers a structural explanation for the extreme potency of D1D2-IgP. These results imply that inter- and intra-virion spike cross-linking may be critical structural determinants of neutralizing potency. It follows that the flexibility of D1D2-IgP, which presumably allows spike cross-linking, may be a more important structural determinant of its potency than steric bulk or polyvalence *per se*.

Monovalent compounds such as BMS-378806 that, like

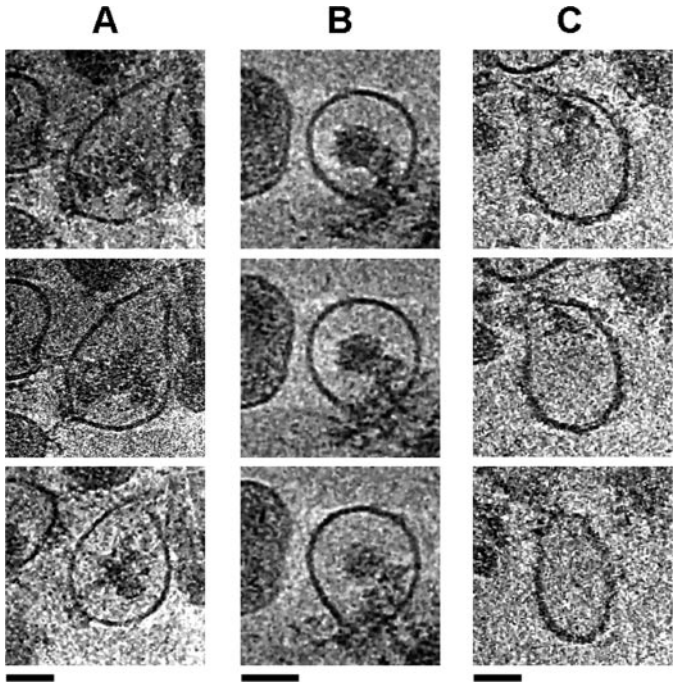

FIGURE 5. **Virion rupture by CD4-mediated D1D2-IgP binding.** Cryoelectron tomographic slices (thickness 8.2 nm) of individual structurally altered SIV virions that have been treated with D1D2-IgP, from tilt series recorded at 300 kV. Columns *A*, *B*, and *C* each show three slices at different depths through the same virion tomogram. *Scale bars*, 50 nm.

D1D2-IgP, bind gp120 at the CD4 binding site have already shown great promise in initial studies (reviewed in Ref. 4). A bivalent version has a 5-fold greater potency *in vitro* (as measured by IC_{90} values) than the monovalent compound, but substantial increases are not seen with polyvalent species based on a rigid scaffold (27). As an extension of the results presented here, we propose that small molecule and low molecular weight gp120 ligands that are both polyvalent and connected on a flexible scaffold may be excellent candidates for effective HIV neutralization in a pharmacologically useful context.

Acknowledgments—We thank Wim Hagen for assistance with maintenance of electron microscopes, Jeffrey Lifson for providing viruses, and Dimiter Dimitrov for helpful discussions.

REFERENCES

1. Dalgleish, A. G., Beverley, P. C., Clapham, P. R., Crawford, D. H., Greaves, M. F., and Weiss, R. A. (1984) *Nature* **312,** 763–767
2. Maddon, P. J., Dalgleish, A. G., McDougal, J. S., Clapham, P. R., Weiss, R. A., and Axel, R. (1986) *Cell* **47,** 333–348
3. Turner, B. G., and Summers, M. F. (1999) *J. Mol. Biol.* **285,** 1–32
4. Kadow, J., Wang, H. G., and Lin, P. F. (2006) *Curr. Opin. Investig. Drugs* **7,** 721–726
5. Daar, E. S., and Ho, D. D. (1991) *Am. J. Med.* **90,** Suppl. 1 22S–26S
6. Kwong, P. D., Doyle, M. L., Casper, D. J., Cicala, C., Leavitt, S. A., Majeed, S., Steenbeke, T. D., Venturi, M., Chaiken, I., Fung, M., Katinger, H., Parren, P. W., Robinson, J., Van Ryk, D., Wang, L., Burton, D. R., Freire, E., Wyatt, R., Sodroski, J., Hendrickson, W. A., and Arthos, J. (2002) *Nature* **420,** 678–682
7. Chen, B., Vogan, E. M., Gong, H., Skehel, J. J., Wiley, D. C., and Harrison, S. C. (2005) *Nature* **433,** 834–841
8. Kwong, P. D. (2005) *Nature* **433,** 815–816
9. Kwong, P. D., Wyatt, R., Robinson, J., Sweet, R. W., Sodroski, J., and Hen-

drickson, W. A. (1998) *Nature* **393,** 648–659
10. Krummel, M. F., Sjaastad, M. D., Wulfing, C., and Davis, M. M. (2000) *Science* **289,** 1349–1352
11. Singer, I. I., Scott, S., Kawka, D. W., Chin, J., Daugherty, B. L., DeMartino, J. A., DiSalvo, J., Gould, S. L., Lineberger, J. E., Malkowitz, L., Miller, M. D., Mitnaul, L., Siciliano, S. J., Staruch, M. J., Williams, H. R., Zweerink, H. J., and Springer, M. S. (2001) *J. Virol.* **75,** 3779–3790
12. Arthos, J., Cicala, C., Steenbeke, T. D., Chun, T. W., Dela Cruz, C., Hanback, D. B., Khazanie, P., Nam, D., Schuck, P., Selig, S. M., Van Ryk, D., Chaikin, M. A., and Fauci, A. S. (2002) *J. Biol. Chem.* **277,** 11456–11464
13. Binley, J. M., Wrin, T., Korber, B., Zwick, M. B., Wang, M., Chappey, C., Stiegler, G., Kunert, R., Zolla-Pazner, S., Katinger, H., Petropoulos, C. J., and Burton, D. R. (2004) *J. Virol.* **78,** 13232–13252
14. Trkola, A., Pomales, A. B., Yuan, H., Korber, B., Maddon, P. J., Allaway, G. P., Katinger, H., Barbas, C. F., III, Burton, D. R., and Ho, D. D. (1995) *J. Virol.* **69,** 6609–6617
15. Chertova, E., Bess, J. W., Jr., Crise, B. J., Sowder, R. C., II, Schaden, T. M., Hilburn, J. M., Hoxie, J. A., Benveniste, R. E., Lifson, J. D., Henderson, L. E., and Arthur, L. O. (2002) *J. Virol.* **76,** 5315–5325
16. Trubey, C. M., Chertova, E., Coren, L. V., Hilburn, J. M., Hixson, C. V., Nagashima, K., Lifson, J. D., and Ott, D. E. (2003) *J. Virol.* **77,** 12699–12709
17. Rossio, J. L., Esser, M. T., Suryanarayana, K., Schneider, D. K., Bess, J. W., Jr., Vasquez, G. M., Wiltrout, T. A., Chertova, E., Grimes, M. K., Sattentau, Q., Arthur, L. O., Henderson, L. E., and Lifson, J. D. (1998) *J. Virol.* **72,** 7992–8001
18. Winkler, H., and Taylor, K. A. (2006) *Ultramicroscopy* **106,** 240
19. Bauer, S., Groh, V., Wu, J., Steinle, A., Phillips, J. H., Lanier, L. L., and Spies, T. (1999) *Science* **285,** 727–729
20. Kolar, G. R., and Capra, J. D. (2003) in *Fundamental Immunology* (Paul, W. E., ed), 5th Ed., Lippincott, Williams, and Wilkins, Philadelphia
21. Hansma, H. G., and Hoh, J. H. (1994) pp. 47–68 *Annu. Rev. Biophys. Biomol. Struct.* **23,** 115–139
22. Zhu, P., Liu, J., Bess, J., Jr., Chertova, E., Lifson, J. D., Grise, H., Ofek, G. A., Taylor, K. A., and Roux, K. H. (2006) *Nature* **441,** 847–852
23. Sougrat, R., Bartesaghi, A., Lifson, J. D., Bennett, A. E., Bess, J. W., Zabransky, D. J., and Subramaniam, S. (2007) *PLoS Pathog.* **3,** e63
24. Zhu, P., Chertova, E., Bess, J., Jr., Lifson, J. D., Arthur, L. O., Liu, J., Taylor, K. A., and Roux, K. H. (2003) *Proc. Natl. Acad. Sci. U. S. A.* **100,** 15812–15817
25. Fazel, S., Wiersma, E. J., and Shulman, M. J. (1997) *Int. Immunol.* **9,** 1149–1158
26. Zhu, P., Olson, W. C., and Roux, K. H. (2001) *J. Virol.* **75,** 6682–6686
27. Wang, J., Le, N., Heredia, A., Song, H., Redfield, R., and Wang, L. X. (2005) *Org. Biomol. Chem.* **3,** 1781–1786
28. Wang, J., Yan, Y., Garrett, T. P. J., Liu, J., Rodgers, D. W., Garlick, R. L., Tarr, G. E., Husain, Y., Reinherz, E. L., and Harrison, S. C. (1990) *Nature* **348,** 411–418
29. Saphire, E. O., Parren, P. W. H. I., Pantophlet, R., Zwick, M. B., Morris, G. M., Rudd, P. M., Dwek, R. A., Stanfield, R. L., Burton, D. R., and Wilson, I. A. (2001) *Science* **293,** 1155–1159
30. Furtado, P. B., Whitty, P. W., Robertson, A., Eaton, J. T., Almogren, A., Kerr, M. A., Woof, J. M., and Perkins, S. J. (2004) *J. Mol. Biol.* **338,** 921–941
31. Kwong, P. D., Wyatt, R., Sattentau, Q. J., Sodroski, J., and Hendrickson, W. A. (2000) *J. Virol.* **74,** 1961–1972